DETERMINING ATMOSPHERIC CONDITIONS AT THE TERMINATOR OF THE HOT JUPITER HD 209458b

David K. Sing,[1] A. Vidal-Madjar,[1] A. Lecavelier des Etangs,[1] J.-M. Désert,[1]
G. Ballester,[2] and D. Ehrenreich[3]
Received 2008 March 7; accepted 2008 May 6

ABSTRACT

We present a theoretical model fit to the *HST* STIS optical transit transmission spectrum of HD 209458b. In our fit, we use the sodium absorption line profile along with the Rayleigh scattering by H_2 to help determine the average temperature-pressure profile at the planetary terminator and infer the abundances of atomic and molecular species. The observed sodium line profile spans an altitude range of $\sim$3500 km, corresponding to pressures between $\sim$0.001 and 50 mbar in our atmospheric models. We find that the sodium line profile requires either condensation into sodium sulfide or ionization, necessary to deplete atomic sodium only at high altitudes below pressures of $\sim$3 mbar. The depletion of sodium is supported by an observed sudden abundance change, from 2 times solar abundance in the lower atmosphere to 0.2 solar or lower in the upper atmosphere. Our findings also indicate the presence of a hot atmosphere near stratospheric altitudes corresponding to pressures of 33 mbar, consistent with that of the observed dayside temperature inversion. In addition, we find that a separate higher altitude temperature rise is necessary within both the condensation and ionization models, corresponding to pressures below $\sim$0.01 mbar. This hot higher altitude temperature indicates that absorption by atomic sodium can potentially probe the bottom of the thermosphere and is possibly sensitive to the temperature rise linked to atmospheric escape.

Subject headings: planetary systems — radiative transfer — stars: individual (HD 209458)

1. INTRODUCTION

Early theoretical transit models of hot Jupiter exoplanetary atmospheres (Seager & Sasselov 2000; Brown 2001; Hubbard et al. 2001) contained strong sodium absorption signatures, predicted to be as high as 0.2% for clear, cloudless atmospheres. The original measured Na absorption signature in HD 209458b from medium-resolution *HST* data (Charbonneau et al. 2002) was, however, $\sim$3 times smaller than the initial predictions. In addition, Barman (2007) has also identified a potential broadband Na signature from photometry of low-resolution STIS data in the same planet, taken several years later (Knutson et al. 2007). These observations have lead to multiple theories explaining the small Na signature. The most widely cited explanations of reduced Na absorption include high clouds or hazes, ionization, low global Na abundance, rainout, and non−local thermal equilibrium effects (Charbonneau et al. 2002; Barman et al. 2002; Barman 2007; Fortney et al. 2003). High opaque clouds could potentially mask absorption features by effectively cutting transit information for altitudes lower than the cloud deck (Seager & Sasselov 2000; Fortney et al. 2003). The small atmospheric signature has made detection from ground-based telescopes difficult, with no Na detection currently reported for HD 209458b after multiple attempts (Narita et al. 2005; Arribas et al. 2006).

In the grazing line of sight of transit geometry, the measured effective altitude depends on the wavelength-dependent opacities of the atmospheric constituents giving a transit transmission spectrum its altitude sensitivity (see relevant equations in Lecavelier des Etangs et al. 2008a). The effective altitude is also dependent on the abundance of absorbing atmospheric particles, as well as the atmospheric pressure. As the abundances are not in general a priori known, this leads to atmospheric models which have degenerate solutions between modeled abundance and pressure, where an atmospheric transit model with increased abundance is identical to models with lower abundances and higher pressures.

Here we interpret the optical *HST* STIS transmission spectra of HD 209458b of Sing et al. (2008). The spectra consist of STIS data obtained during planetary transit at low and medium spectral resolutions. The two data sets are combined to extend the measurements over the entire optical regime, providing a way to simultaneously measure, in the case of atomic Na, both the narrow line core and wide line wing absorption, as well as other absorbing or scattering species. Since the Na line core and wings are optically thick at different atmospheric heights, a detailed analysis of the Na line profile in conjunction with other observed species can potentially break the model degeneracies and reveal atmospheric structure such as the altitude-temperature-pressure (*z-T-P*) relation, abundance, and the possible presence and height of planetary clouds. In this paper, we focus mainly on the resulting temperature-pressure profile, as well as the Na line itself. We briefly describe the observations and resulting spectra in § 2, present our transit model fits in § 3, report on an observed temperature inversion in § 3.3, and discuss our results in §§ 4 and 5. In addition to this work, Lecavelier des Etangs et al. (2008b) provide a detailed description of H_2 Rayleigh scattering, while Désert et al. (2008) go into modeling details of TiO, VO, and other molecular species.

2. OBSERVATIONS

The data reduction, procedures, and various tests resulting in the transmission spectra used in this analysis are covered in detail by Sing et al. (2008), although we briefly describe them here for completeness. The *HST* STIS optical transit data for HD 209458b consist of data at low resolution covering $\sim$3000−10000 Å with the G430L and G750L gratings and medium-resolution data from the G750M grating covering 5813−6382 Å.

With the medium-resolution data, Sing et al. (2008) measured the Na absorption using the double differential photometric method of Charbonneau et al. (2002), as well as a double differential spectroscopic evaluation. For the differential photometric measurement,

[1] Institut d'Astrophysique de Paris, CNRS, Université Pierre et Marie Curie, 98 bis Boulevard Arago, F-75014 Paris, France; sing@iap.fr.
[2] Lunar and Planetary Laboratory, University of Arizona, Sonett Space Science Building, Tucson, AZ 85721-0063.
[3] Laboratoire d'Astrophysique de Grenoble, Université Joseph-Fourier, CNRS (UMR 5571), BP 53, F-38041 Grenoble Cedex, France.
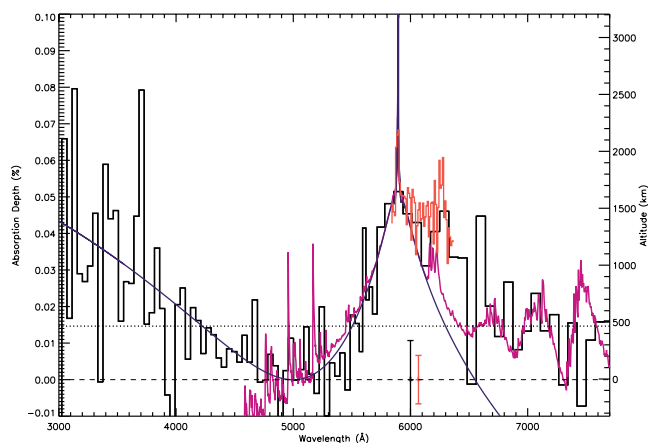
FIG. 1.—Transit Na D absorption from Sing et al. (2008). Plotted is the planetary absorption percentage compared to the minimum absorption level referenced at 5000 Å (1.440%). In black are the low-resolution data binned over 16 pixels, and overplotted in red are the medium-resolution data binned over 18 pixels (10 Å). Representative error bars for the binned data are also plotted (also see Figs. 10 and 11 of Sing et al. 2008), as well as the mean planetary radius from Knutson et al. (2007; *dotted line*). Plotted in blue is our transit absorption model, which contains opacity from atomic Na, Rayleigh scattering, and upper atmospheric Na depletion. The model in purple includes Na, TiO, and VO illustrating the wavelengths where those features are prominent. Higher absorption values indicate higher atmospheric altitudes, with the right *y*-axis labeled as the altitude above our minimum absorption depth, assuming the system parameters of Knutson et al. (2007). The Na D line cores can easily be seen in the zoomed plot of Fig. 2. The narrow Na D1 and D2 cores extend above a wide plateau of Na absorption, indicating that a low amount of Na is present in the middle atmosphere compared to the lower. The drastic abundance change, along with the pressure and temperature where the change occurs, indicates that Na is condensing into sodium sulfide on the night side of the planet.

Sing et al. (2008) selected 23 wavelength bands from 4 to 100 Å centered on the Na D lines. Charbonneau et al. (2002) used three different wavelength bands and compared the absorption to that of regions redward and blueward of the Na D line region. The resulting photometric Na absorption profile (see Fig. 3 of Sing et al. 2008) matches the original results of Charbonneau et al. (2002) and, in addition, reveals the strong absorption from the Na D line centers.

To analyze the low- and medium-resolution *HST* spectra together, Sing et al. (2008) used a limb-darkened corrected transit spectral ratio to probe the full wavelength dependence of atmospheric absorption features (see Figs. 1 and 2). From this analysis, the Na D wavelength region shows an absorption plateau between ∼5600 and 6700 Å, which is ∼0.045% above the minimum absorption level observed (see Fig. 1). Note that the wavelength range of the medium-resolution data, originally used to detect atmospheric Na (Charbonneau et al. 2002), is entirely contained within this broad plateau absorption region. The total absorption seen in the Na D line cores, therefore, is the result from the medium-resolution data, which is the absorption above the plateau region measured to be ∼0.065%, *plus* the absorption level of the plateau region itself. This total Na core absorption level is ∼0.11%, within a 4.4 Å band, and is much closer to the original predictions (Seager & Sasselov 2000; Brown 2001), indicating that a large part of the atmosphere is being probed during transit. In addition, the Na D doublet is resolved in our resulting spectra, which show two strong, narrow absorption lines (see Fig. 2).

2.1. *Observed* Na *Line Profile*

The observed Na D transit line profile (Fig. 1), with its narrow absorption core and broader plateau-like shape, is in stark contrast to cloudless theoretical models of HD 209458b (Seager &
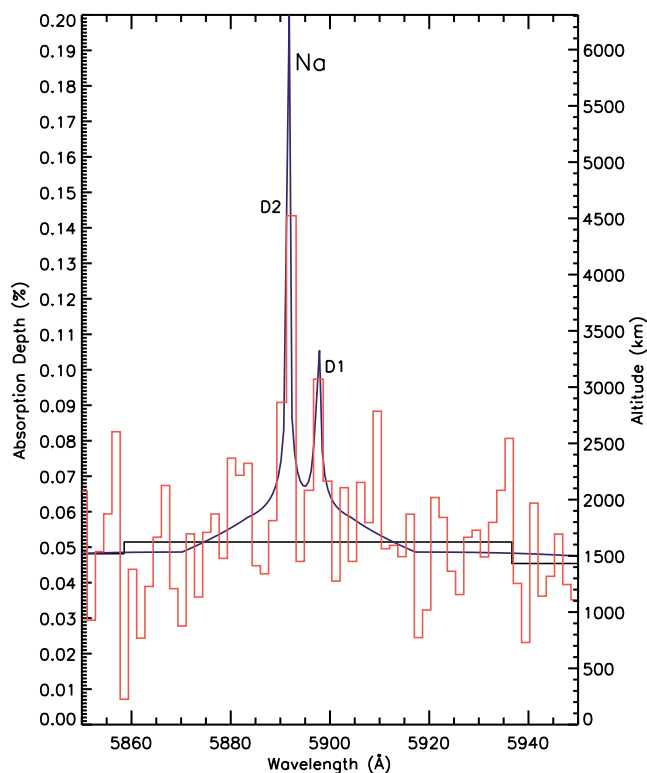

FIG. 2.—Same as Fig. 1, but zoomed on the Na region with the medium-resolution data binned over 3 pixels (1.7 Å). The Na D doublet is easily resolved and reaches up to an average altitude of ∼3500 km.

Sasselov 2000; Brown 2001; Fortney et al. 2003; Barman 2007), which have smoothly decaying Lorentzian "Eiffel Tower"–shaped line wings. This more complicated observed line profile suggests that a very low quantity of Na is present in the middle atmosphere and a much larger quantity in the lower atmosphere, pointing to either high-altitude Na condensation into Na_2S or, alternatively, depletion via ionization.

Previous studies have predicted models of HD 209458b which included Na_2S clouds (Iro et al. 2005), as high-altitude temperatures on the night side reach levels cool enough for condensation of atomic Na (Lodders 1999; Showman & Guillot 2002). Sodium sulfide would effectively decrease the amount of atomic sodium at altitudes above the condensation temperature, creating a stratified atmospheric profile depleted of atomic Na only at those high altitudes. The transit signature with such a layered Na profile produces a broad plateau-shaped line wing along with narrow absorption cores rising above the plateau to higher levels (Iro et al. 2005). Na_2S would have to be transparent, since it is not observed in absorption during transit at the limb. If Na_2S or other clouds/hazes were opaque in absorption during transit at the condensation altitude, significant absorption would extend over a very broad wavelength range (Fortney 2005), masking the low-resolution absorption features we observe. Such a flat, largely featureless transmission spectrum has recently been observed in HD 189733b, the result of high-altitude haze (Pont et al. 2008; Lecavelier des Etangs et al. 2008a).

An alternative method to deplete neutral atomic sodium is ionization (Fortney et al. 2003). In this scenario, UV photons between wavelengths of 1107 and 2412 Å (corresponding to 11.2 and 5.14 eV, respectively) photoionize sodium along the transit line of sight until recombination matches ionization. Fortney et al. (2003) found a sharp boundary at the limb between higher atmospheric regions of complete ionization and lower regions with no ionization.

Such a model could explain the observed Na line shape, with a narrow Na absorption core rising above broad line wings, if the atmosphere suddenly becomes ionized above a certain altitude.

3. MODEL FITS TO THE TRANSIT TRANSMISSION SPECTRA OF HD 209458b

We modeled the atmospheric transmission spectra calculating the transit signature based on a theoretical model (Ehrenreich et al. 2006) containing absorption by Na, H_2 Rayleigh scattering, TiO, and VO. The model output absorption spectrum can then be directly compared to our limb-darkened corrected transit absorption spectrum. We calculated the optical depth along a grazing line of sight through the planet's atmosphere and the absorption depth at a given wavelength using equations given in Lecavelier des Etangs et al. (2008a). For the Na D lines, we used collision-broadened line shapes calculated using the equations of Iro et al. (2005). Concerning atomic sodium, ultimately, the free parameters that fit into the transit calculation include the atmospheric temperature profile as a function of altitude and the mixing ratios of Na below and above the condensation or ionization level (see Fig. 3).

We found two families of solutions, with each giving similarly good fits to the data. In one model Na is allowed to condense into sodium sulfide at the chemical equilibrium temperature, while in the other model neutral Na is depleted at high altitudes, presumably by ionization, below an arbitrary pressure.

3.1. Condensation Model

3.1.1. Temperature-Pressure Profile

For the calculation, we fit various simplified T-P profiles in which the temperature is taken as a linear function of the altitude and pressure is calculated using hydrostatic equilibrium. Note that it is not specifically the T-P profile shape itself which is important in our fitting of the data, but rather the different temperature and pressure regimes imposed by the observations. At our signal-to-noise (S/N) levels, the general variation of the T-P profile between the different atmospheric regimes we find (hot at high pressures, cool at middle pressures, and hot at low pressures) is only loosely constrained. A more complicated T-P profile would add undesired additional parameters into the fit, leading us to choose as simple a T-P profile as possible.

We found it necessary to have a minimum of three variable points in the T-P profile. The temperature as a function of the altitude, $T(z)$, is thus composed of two linear functions below and above the altitude z_m, where z_m is the altitude of the minimum temperature, T_m. We took the lower reference altitude, z_s, for the altitude corresponding to the mean planetary radius (Knutson et al. 2007), and the altitude z_{th} is the fixed position, at high altitude, needed to define the second part of the $T(z)$ linear function. We used z_{th} corresponding to the altitude of the absorption depth of 1.55%, which corresponds to the mean absorption depth in the core of the sodium doublet. The temperature and pressure at the altitude z_s, the altitude z_m of minimum temperature T_m, and T_{th} are three of the five free parameters defining the T-P profile. The sodium abundances in the lower and upper atmosphere are the two other free parameters in the fit.

In our condensation fit we found (1) a high temperature of 2200 ± 260 K at 33 ± 5 mbar ($\sim$500 km) mainly constrained by Rayleigh scattering (Lecavelier des Etangs et al. 2008b) seen at wavelengths shorter than $\sim$5000 Å, (2) a low temperature of 420 ± 190 K at 0.63 ± 0.27 mbar needed to explain the plateau at 0.045% ($\sim$1500 km) above the minimum absorption level as a Na abundance change due to condensation, and, finally, (3)
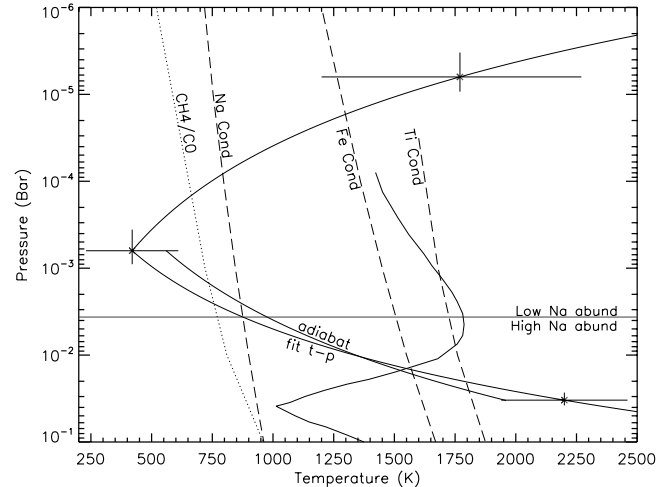

Fig. 3.—Limb temperature-pressure atmospheric profile of HD 209458b for the sodium condensation model. Plotted (*thick line, three points with error bars*) is our best-fit terminator T-P profile, while the thin line shows a dayside inverted profile from Burrows et al. (2007). Also shown are the chemical equilibrium condensation curves of iron, TiO, and sodium (*dashed lines*). The horizontal line represents the pressure at which the T-P profile crosses the sodium condensation curve. Above the condensation curve, at high altitudes and low pressures, Na is depleted compared to lower altitudes. The CH4/CO line represents the profile where equal amounts of CO and CH4 are expected, assuming chemical equilibrium. The whole data set with low- and medium-resolution observations is fitted with a total of seven free parameters, resulting in the plotted T-P profile and sodium abundance below and above the sodium condensation temperature. A fit imposing an adiabatic lower T-P profile is also shown. The sodium abundance above the Na_2S condensation level is found to be significantly lower than the sodium abundance below the condensation level (the ratio of both abundances is significantly above 1 at the 3 σ level); this reveals the presence of Na_2S condensation.

a high-altitude ($\sim$3500 km) high temperature of 1770^{+500}_{-570} K at 0.0063 ± 0.003 mbar needed to fit the strong peak and narrow width of the cores of the Na I doublet.

The pressure-temperature gradient we find when imposing condensation is close to and consistent with (within 1 σ) an adiabatic gradient. To be stable against convection, a temperature gradient which is adiabatic or less is needed, and solutions imposing adiabatic variations give acceptable fits to the data (an adiabatic fit is shown in Fig. 3). We ultimately, however, choose to quote values found from the more general solution, as the linear temperature-altitude relation we assume includes adiabatic gradients and the general fit is located at a well-behaved minimum χ^2. Although the best-fit solution is slightly superadiabatic, the relatively low quality of the data still allows for a wide range of T-P gradients, and the adiabatic profile found from our general fit indicates that adiabatic behavior is likely at those altitudes.

3.1.2. Atmospheric Na Condensation, TiO, and VO

Our model contained two different amounts of atomic Na with separate variable parameters for the mixing ratios of the middle and lower atmospheres. The pressure boundaries (or condensation pressure) where the quantity changes occur is taken to be at an altitude where the temperature profile crosses the Na_2S condensation curve. In our fits, we found a Na mixing ratio of $3.5^{+2.9}_{-1.9} \times 10^{-7}$ in the middle atmosphere and $4.3^{+2.1}_{-1.9} \times 10^{-6}$ in the lower atmosphere, corresponding to 0.2 and 2 times solar abundance.

Fortney (2005) estimated that the optical depth of Na_2S condensates in transit geometry could be optically thick for HD 209458b ($\tau \sim 0.73$) for an atmosphere of solar composition and cloud base at 30 mbar. Given the fitted T-P profile, we find a Na_2S cloud base of $\sim$3 mbar. Lower pressures or larger particle sizes would provide a natural explanation for transparent clouds,

as the condensate optical depth is proportional to the pressure and inversely proportional to the particle size (Marley 2000). Given our determined Na abundances, the mixing ratio of Na_2S we find is $(2 \pm 1) \times 10^{-6}$, which matches the assumed value of Fortney (2005). Scaling the estimated optical depth of Fortney (2005), a cloud base at 3 mbar gives $\tau \sim 0.073$, indicating that transparent Na_2S condensates are plausible.

The continuum blueward of the Na D lines, between ~4000 and 5500 Å, shows a slightly lower absorption than the redward region, 7000–8000 Å, and a significant absorption "bump" around ~6250 Å which appears in both resolutions. Our fits indicate that the redward absorption levels (7000–8000 Å) are likely due to TiO and VO at stratospheric heights, being largely confined to altitudes below our Na condensation level (also see Désert et al. 2008). The TiO and VO features mask part of the long-wavelength Na line wing, although not the short-wavelength side, providing strong constraints on the abundance and altitude of TiO and VO. The hot low-altitude temperatures we find from Rayleigh scattering are consistent with the presence of TiO and VO, as both species begin to condense out of the atmosphere at temperatures below ~1800 K.

The low-altitude pressure assumed here is dependent on the detection of Rayleigh scattering (Lecavelier des Etangs et al. 2008b), although multiple interpretations of the absorption rise at those wavelengths exist (Lecavelier des Etangs et al. 2008b; Ballester et al. 2007; Barman 2007). Ultimately, it may be difficult without Rayleigh scattering to assign an absolute pressure scale to these measurements, which are inherently differential. The effective planetary radius seen during transit is sensitive to the quantity of the atmospheric pressure times the abundance of absorbing species (see equations of Lecavelier des Etangs et al. 2008a), making an atmospheric fit at higher altitude possible by simply increasing the absorber abundance. The advantage of detecting Rayleigh scattering by H_2 when interpreting these models is that the abundance of H_2 is known, constituting the bulk of the atmosphere, which thereby fixes the pressure and defines the pressure scale for the rest of the transmission spectrum. Our adoption of Rayleigh scattering here is based on the goodness of fit to the data and the necessity of probing a large pressure range, given the total Na profile observed.

Since the low-altitude pressure is an upper limit constrained by Rayleigh scattering, a lower pressure would have an effect on the lower temperature profile, increase the lower Na mixing ratio, and decrease the condensate pressure determined in our transit fit. Whatever the true pressure P_s or additional absorption sources, however, the basic atmospheric characteristics of Na determined here would remain the same. Namely, the middle atmosphere has a greatly reduced amount of Na with a temperature below Na_2S condensation, while the lower and higher atmospheres are warmer than the condensation temperature, with the lower atmosphere containing a solar-like Na abundance and the higher one a significantly reduced Na abundance.

3.2. Photoionization Model

Given the large uncertainties of modeling hot Jupiter Na photoionization, we choose not to employ a complex ionization model, but rather follow the results of Fortney et al. (2003) and assume in our model that neutral Na can be suddenly ionized above a given altitude, leading to the observed Na depletion. The ionization depth found by Fortney et al. (2003) is around 1.7 mbar, close to the pressure we find for a Na abundance change in the condensation model, indicating that the effects could be important at those pressures and such a model is viable.

A model with Na ionization effectively lifts the constraint of the temperature profile dropping below the Na condensation curve, which the condensation model uses to deplete atomic Na. Effectively, a model with Na ionization leaves a wide range of temperatures possible in the middle atmosphere (corresponding in our model to T_m), as the collisionally broadened Na profile at those altitudes (1000–2000 km) contains no temperature information. The corresponding H_2 Rayleigh scattering slope (below ~3400 Å) is at the edge of the spectrum and also provides no useful middle-atmospheric temperature constraints. Within the framework of equilibrium chemistry, the temperature T_m is likely below that of the TiO/VO condensation curve and above that of the Na_2S condensation curve. However, Rayleigh scattering still implies a high temperature of 2200 ± 260 K at 33 ± 5 mbar, and the deep, narrow Na cores suggest high-altitude temperatures of around 1770^{+500}_{-570} K. Without a strong constraint on the middle-atmosphere temperature, T-P profile fits are dominated by these upper and lower atmospheric constrains, leading to anomalously high-temperature T-P profiles fit to be everywhere above 2000 K. Although technically good fits to the data, such profiles can be ruled out, as everywhere the temperatures would be higher than the dayside temperature inversion seen with *Spitzer* (Knutson et al. 2008; Burrows et al. 2007). In addition, the lack of observed Ca I at 4227 Å in the low-resolution data further suggests temperatures reach values lower than that required for Ca-Ti and Ca-Al-bearing condensates (Lodders & Fegley 2006).

Though the current data lack enough constraints for a unique T-P profile solution in the photoionization model, the ionization pressure, P_{ion}, can be estimated given the likely range of temperatures. We fit various isothermal models fitting P_{ion} as a free parameter along with the Na abundances (taken to be constant) above and below that pressure. The resulting ionization pressure varies from 0.5 to 5 mbar for temperatures of 1100 and 2000 K, respectively. Higher temperature fits result in smaller upper atmospheric Na abundances and larger Na abundance contrasts. The abundances found in the lower temperature fits are in general agreement with those found in the Na condensation model, while the upper temperature fits find much smaller upper abundances, with the 2000 K model giving an upper Na abundance 180 times less than solar. Thus, a Na abundance drop by a factor of 10 can be considered as a lower limit and may be much larger depending on the depletion mechanism.

3.3. High-Altitude Temperature Inversion

An $\sim0.11\%$ absorption of Na indicates that our transmission spectra probe an altitude range of ~3500 km. Such a large altitude range with our slant transit geometry indicates that we are sensitive to pressures between tens of mbar and ~0.001 mbar. These limb pressures are in agreement with those found from Fortney et al. (2003), who analyzed the original Charbonneau et al. (2002) medium-resolution Na measurements. At pressures higher than 30–50 mbar, our transmission spectra are optically thick to Rayleigh scattering by the abundant molecule H_2, providing a firm upper pressure limit. Such pressure restrictions, in addition to the strong narrow Na line cores, facilitate the necessity of a hot high-altitude temperature (above ~1500), which then naturally provides the observed altitude range due to an increased scale height. Our high-altitude high-limb temperature may point toward the atmospheric escape mechanism being felt, which necessitates large temperature rises to perhaps 10,000 or 15,000 K in the exosphere (Yelle 2004; Vidal-Madjar et al. 2003, 2004).

The highest altitudes probed here are dependent on the Na core, however, and thus have a correspondingly larger associated error.
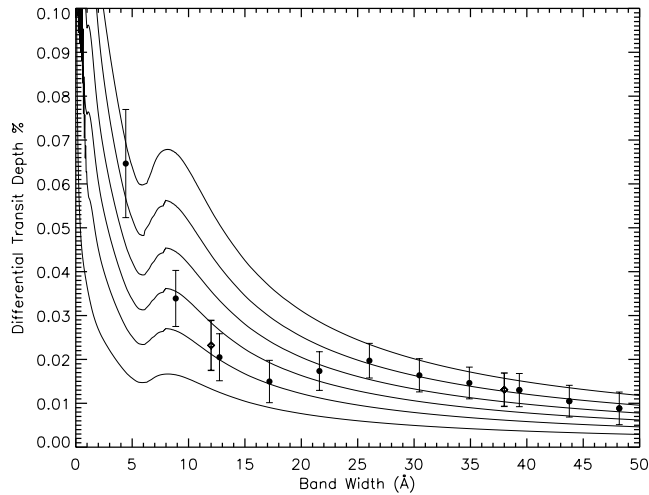
Fig. 4.— Differential spectrophotometric measurements of atmospheric sodium absorption from Charbonneau et al. (2002; *diamonds*) and Sing et al. (2008; *circles*) using the *HST* STIS medium-resolution data. Also plotted are the Na absorption predictions from isothermal models with temperatures (*bottom to top*) of 500, 750, 1000, 1250, 1500, and 2000 K and constant sodium abundance. The isothermal models illustrate the necessity of a high-altitude temperature increase in the narrowest two photometric bands (4.4 and 8.9 Å) which probe the highest altitudes.

The large error coupled with the possible Na depletion mechanisms leaves open a wide range of possible upper atmospheric temperature profiles. However, a high-altitude temperature rise can be seen when analyzing the narrowest Na wavelength bands alone, sensitive to high altitudes well above the condensation/ionization altitude, making the high-altitude temperature measurement independent of the depletion mechanism. The hot high-altitude temperature is illustrated in Figure 4, which shows photometric Na measurements from Charbonneau et al. (2002) and Sing et al. (2008) overplotted with various constant abundance isothermal models. A single isothermal model fits through the 12 and 17 Å bands, indicating that the temperature and Na abundance do not change significantly between those altitudes ($\sim$2000–2200 km). However, the absorptions measured in the 4.4 and 8.9 Å bands, which probe higher in altitude ($\sim$2700–3700 km), rise much faster than the isothermal model fitting the lower altitudes of the 12 and 17 Å bands, indicating that warmer temperatures are needed.

In the ionization Na depletion scenario, there are less temperature constraints for the middle atmosphere compared to the Na condensation model. However, limb temperatures everywhere above $\sim$1500 K are unlikely and in contradiction with *Spitzer* measurements of infrared brightness temperature. The *T-P* profiles applicable to Na ionization models have less severe temperature rises compared to the condensation model, although a hot high-altitude temperature is still necessary and at least a modest temperature rise probable.

A similar high-altitude temperature rise will also likely be necessary to explain recent measurements of another hot Jupiter, HD 189733b. The Na core in that hot Jupiter reaches $\sim$4950 km above the average optical transit altitude (Redfield et al. 2008; Pont et al. 2007). As the atmospheric scale height of HD 189733b is smaller than that of HD 209458b at the same temperature, a more extreme high-altitude temperature rise is likely necessary to fully explain the existing measurements.

3.4. *Comparison with Spitzer Antitransit Data*

A stratospheric temperature inversion has been used to interpret *Spitzer* infrared secondary eclipse measurements of HD 209458b

(Knutson et al. 2008), thought to be caused by an absorber at optical wavelengths on the day side of the planet (Burrows et al. 2007; Fortney et al. 2008). This optical absorber has been postulated to be clouds or molecules of TiO and VO (Hubeny et al. 2003; Burrows et al. 2007; Fortney et al. 2008), with a low albedo ruling out some species, although not TiO or VO (Rowe et al. 2006; Burrows et al. 2007).

Comparing our limb *T-P* profile to the dayside profile from Burrows et al. (2007; see Fig. 3), the atmospheric pressures probed are similar, between 0.01 and 30 mbar, despite our slant transit viewing geometry (Fortney 2005). The atmosphere in the infrared has a higher opacity, due to strong molecular transitions from species such as water (Burrows et al. 2007), placing the infrared surface of the planet viewed at normal angles at altitudes similar to those probed in slant geometry in the optical at the limb.

The high-altitude temperature inversion we observe at the limb below pressures of $\sim$1 mbar is separate from that of the day side and occurs at a much higher altitude. However, the altitude of TiO and VO we find from both models, largely confined to pressures above $\sim$10 mbar, closely matches the model presented by Burrows et al. (2007), who placed the stratospheric absorber at pressures of $\sim$25 mbar and imposed heat redistribution between pressures of 10 and 100 mbar. The probable presence of TiO and VO in our spectrum along with the altitude similarity implies that TiO and VO are indeed likely to be the stratospheric dayside temperature inversion instigators (Fortney et al. 2008). As our fit of TiO and VO is based largely on low-resolution data, a more robust detection and interpretation of TiO/VO will likely require higher resolution *HST* spectra than those used here, such that multiple specific molecular band heads can be observed.

Some form of heat redistribution at or near our low-altitude pressure ($\sim$30 mbar) would likely be needed to explain the high temperature we find there, as the temperatures there are significantly above that predicted by radiative equilibrium (Showman et al. 2008). Initial *Spitzer* mid-infrared measurements of the brightness temperature as a function of orbital phase have revealed that at least 30% of the energy from the stellar flux must be redistributed to the night side to explain their null results, implying efficient heat redistribution (Cowan et al. 2007). Comparing with models by Burrows et al. (2007, 2008) with higher P_n values ($>$0.35), nightside temperatures in the region of imposed heat distribution (corresponding to our pressure at z_s) can have larger temperatures than the day side, perhaps explaining our high temperature at z_s. Alternatively, systematic pressure scale differences between the two studies may indicate that our transmission spectra instead probe the top of the stratospheric temperature inversion, giving a potential explanation of the high temperature at z_s, as those altitudes could already be warm. The minimum temperature we find, however, is in general agreement with radiative equilibrium, perhaps implying that the approximation is valid at those pressures around 1 mbar. Such scenarios can be further distinguished in future studies, with tighter constraints on the average infrared and optical opacities, additional infrared observations, and improved global circulation models. The presence of a temperature inversion, TiO, and VO, along with heat redistribution, would seem to currently place HD 209458b in a intermediate hot Jupiter class between the pM and pL classes as proposed by Fortney et al. (2008).

4. DISCUSSION

The atmospheric temperatures we find within the condensation scenario and the presence of TiO and VO can also explain other HD 209458b observational features. For instance, the low

middle-atmospheric temperature and the presence of TiO and VO would also explain the lack of observed potassium (K), originally predicted to be a major contributor to the optical opacity. At the lower temperatures of the middle atmosphere, K condenses into potassium chloride, allowing KCl to become a dominant K-bearing gas. Condensed K would then naturally deplete the atmosphere of atomic K, as seen here with Na, leading to reduced signatures. In the lower warmer atmosphere, where wide atomic K line wings would be observable even at low resolution, TiO and VO likely make up the surrounding continuum, further masking the signature. If Na is instead ionized, the minimum limb temperature is higher, and ionization of K, which is easier than Na to ionize, likely depletes neutral K. If present in the atmosphere, a positive detection of atomic K in HD 209458b will probably require high-resolution ground-based or medium-resolution space-based data to detect the K line core. Further detections or upper limits of other atomic species which have different ionization potentials and condensation temperatures can offer clues in future studies when distinguishing between the two depletion scenarios.

The Na mixing ratio we find for the lower atmosphere is about 2 times solar, while the abundance in the middle and upper atmosphere is found to be 0.2 times solar or less; thus, our models have decreased Na abundance without the need for a global deficiency of Na. In chemical equilibrium, Na_2S condensation effectively removes all the Na below the condensation temperature, since the protosolar Na abundance is ~13% that of S, limiting the amount of Na_2S which can condense directly to the amount of Na. Our condensation model T-P profile crosses the condensation curve again at higher altitude, making the altitudes of our minimum temperature a "cold trap" for Na. It is currently unclear how the second crossing of the condensation curve could affect the Na abundance, as the S/N limits us to fitting only a single value for the whole upper Na abundance.

Assuming equilibrium chemistry, our temperature profile would also result in less CO in the middle atmosphere, as our temperature profile at that level is closer to the $CO = CH_4$ curve, which would result in an enhancement of CH_4 and H_2O over that of CO and H_2 (see Fig. 2). This is consistent with the lack of CO detection in HD 209458b during transit (Deming et al. 2005), although deviations from equilibrium have been shown to push the CH_4/CO ratio to small values for the pressures probed here of less than 1 bar (Cooper & Showman 2006).

Atmospheric data resulting from transit measurements represent the average atmospheric properties across the observed limb of the planet, which would include the morning, evening, and pole terminators. As previously recognized by Iro et al. (2005), temperature and structure differences could result in differing transit signatures between the morning and evening terminators. Longitudinal differences might also play a role, although the transit geometry generally limits significant opacity contributions to regions of the terminator itself, as the density drops rapidly from the terminator along the transit line of sight (Hansen 2008). A T-P profile decreasing in temperature and pressure with increasing altitude would further mitigate longitudinal differences, corresponding to pressures above 1 mbar in our condensation model fit. Efficient heat redistribution (Cowan et al. 2007) implies that all these differences could be minimal, although future Spitzer observations and the next generation of global climate models would be able to better quantify the differences. Given the size of our temperature uncertainties, limb differences of even several hundred degrees would have a negligible impact on our resulting model fit.

Primary transit data alone are currently not able to give detailed knowledge on atmospheric differences between the morning and evening terminators. Such transit signatures would appear during ingress and egress, where the transit light curve is less sensitive to changes in planetary radii and more sensitive to errors in limb-darkening. Nevertheless, as our Na D line cores remain relatively narrow in the medium-resolution data, sensitive to the middle and upper atmospheres, a solar abundance of Na on the potentially warmer evening terminator in the middle and upper atmospheres is ruled out. For the condensation model, this would indicate that Na settles from the middle atmosphere and remains at lower altitudes, presumably at the Na_2S condensation altitude. Condensed Na_2S would have little impact on antitransit observations and the observational constraint of a low albedo (Rowe et al. 2006). On the day side, the hotter temperatures would sublimate Na_2S back into their atomic constituents and are likely transparent in normal viewing geometry anyway (Fortney 2005).

5. CONCLUSIONS

As seen here, fitting primary transit transmission spectra can give detailed atmospheric information over large altitude ranges, and thus large pressure regimes, where different physical processes may be important. In our case, strong sodium absorption coupled with a relatively clear atmosphere provides this large altitude range and reveals the pressure at which Na depletion via condensation or ionization takes place. The depletion level naturally provides a contrast between the warmer, deeper atmosphere, likely sensitive to global circulation, and a cooler, middle atmosphere where many atomic and molecular species have condensed out and/or are depleted via ionization. Strong opacity in the core of the Na line permits measurements to very low pressures, allowing Na to be sensitive to altitudes perhaps as high as the lower thermosphere. The slant transit geometry and high associated column density restrict the lowest altitudes probed, however, limiting this study to altitudes at and above the stratosphere.

Interpreting transit spectra becomes easier with increased wavelength coverage and resolution. For HD 209458b, low-resolution data spanning the optical reveal a planetary continuum comprised of H_2 Rayleigh scattering, sodium absorption, and TiO/VO, giving a self-consistent picture of a hot atmosphere at pressures around 10 mbar. This result is consistent with infrared Spitzer emission features and a temperature inversion at those altitudes. The medium-resolution data place the detection of Na absorption on firm ground, as there is sufficient S/N and resolution to both resolve the Na doublet and observe the depletion level. This overall atmospheric picture is not possible without data from all three spectroscopic gratings and highlights the importance of future observations at other wavelengths and resolutions.

Transit transmission spectra have become a powerful method to probe the abundances of atomic and molecular species for hot Jupiters, as seen here for HD 209458b and in Swain et al. (2008) for HD 189733b. Both Jupiter and Saturn are enhanced in metals relative to the Sun, as would seem to be the case here for HD 209458b, with a sodium abundance about twice that of its parent star. Such studies can begin to answer the question of whether all hot Jupiters are enriched in heavy elements, shedding light on giant planet formation.

After the next servicing mission, HST will be capable of extending the transmission spectra of HD 209458b from the UV to near-IR, potentially linking important physical atmospheric processes such as the altitude dependence of UV/near-UV energy deposition, as well as abundance and altitudes of other atomic and molecular species. As a patchwork of such observations currently exists for the two ideal targets HD 209458b and HD 189733b,

future observations should focus on covering wavelength and resolution gaps, which can lead to both theoretical and observational links between the separate studies.

REFERENCES

Arribas, S., Gilliland, R. L., Sparks, W. B., Lopez-Martin, L., Mediavilla, E., & Gomez-Alvarez, P. 2006, PASP, 118, 21
Ballester, G. E., Sing, D. K., & Herbert, F. 2007, Nature, 445, 511
Barman, T. S. 2007, ApJ, 661, L191
Barman, T. S., Hauschildt, P. H., Schweitzer, A., Stancil, P. C., Baron, E., & Allard, F. 2002, ApJ, 569, L51
Brown, T. M. 2001, ApJ, 553, 1006
Burrows, A., Budaj, J., & Hubeny, I. 2008, ApJ, 678, 1436
Burrows, A., Hubeny, I., Budaj, J., Knutson, H. A., & Charbonneau, D. 2007, ApJ, 668, L171
Charbonneau, D., Brown, T. M., Noyes, R. W., & Gilliland, R. L. 2002, ApJ, 568, 377
Cooper, C. S., & Showman, A. P. 2006, ApJ, 649, 1048
Cowan, N. B, Agol, E., & Charbonneau, D. 2007, MNRAS, 379, 641
Deming, D., Brown, T. M., Charbonneau, D., Harrington, J., & Richardson, L. J. 2005, ApJ, 622, 1149
Désert, J.-M., Vidal-Madjar, A., Lecavelier des Etangs, A., Sing, D. K., Ehrenreich, D., Hébrard, G., & Ferlet, R. 2008, A&A, submitted
Ehrenreich, D., Tinetti, G., Lecavelier Des Etangs, A., Vidal-Madjar, A., & Selsis, F. 2006, A&A, 448, 379
Fortney, J. J. 2005, MNRAS, 364, 649
Fortney, J. J., Lodders, K., Marley, M. S., & Freedman, R. S. 2008, ApJ, 678, 1419
Fortney, J. J., Sudarsky, D., Hubeny, I., Cooper, C. S., Hubbard, W. B., Burrows, A., & Lunine, J. I. 2003, ApJ, 589, 615
Hansen, B. M. S. 2008, ApJ, submitted (arXiv: 0801.2972)
Hubbard, W. B., Fortney, J. J., Lunine, J. I., Burrows, A., Sudarsky, D., & Pinto, P. 2001, ApJ, 560, 413
Hubeny, I., Burrows, A., & Sudarsky, D. 2003, ApJ, 594, 1011
Iro, N., Bézard, B., & Guillot, T. 2005, A&A, 436, 719

Knutson, H. A., Charbonneau, D., Allen, L. E., Burrows, A., & Megeath, S. T 2008, ApJ, 673, 526
Knutson, H. A., Charbonneau, D., Noyes, R. W., Brown, T. M., & Gilliland, R. L. 2007, ApJ, 655, 564
Lecavelier des Etangs, A., Pont, F., Vidal-Madjar, A., & Sing, D. K. 2008a, A&A, 481, L83
Lecavelier des Etangs, A., Vidal-Madjar, A., Désert, J. M., & Sing, D. K. 2008b, A&A, 485, 865
Lodders, K. 1999, ApJ, 519, 793
Lodders, K., & Fegley, B., Jr. 2006, in Astrophysics Update, Vol. 2, ed. J. W. Mason (Chichester: Praxis), 1
Marley, M. S. 2000, in ASP Conf. Ser. 212, From Giant Planets to Cool Stars, ed. C. A. Griffith & M. S. Marley (San Francisco: ASP), 152
Narita, N., et al. 2005, PASJ, 57, 471
Pont, F., Knuston, H., Gilliland, R. L., Moutou, C., & Charbonneau, D. 2008, MNRAS, 385, 109
Pont, F., et al. 2007, A&A, 476, 1347
Redfield, S., Endl, M., Cochran, W., & Koesterke, L. 2008, ApJ, 673, L87
Rowe, J. F., et al. 2006, ApJ, 646, 1241
Seager, S., & Sasselov, D. D. 2000, ApJ, 537, 916
Showman, A. P., Cooper, C. S., Fortney, J. J., & Marley, M. S. 2008, ApJ, 682, 559
Showman, A. P., & Guillot, T. 2002, A&A, 385, 166
Sing, D. K., Vidal-Madjar, A., Désert, J.-M., Lecavelier des Etangs, A., & Ballester, G. 2008, ApJ, 686, 658
Swain, M. R., Vasisht, G., & Tinetti, G. 2008, Nature, 452, 329
Vidal-Madjar, A., Lecavelier des Etangs, A., Désert, J.-M., Ballester, G. E., Ferlet, R., Hébrard, G., & Mayor, M. 2003, Nature, 422, 143
Vidal-Madjar, A., et al. 2004, ApJ, 604, L69
Yelle, R. 2004, Icarus, 170, 167